How Resilient Are They? Robustness Analysis of LEO Satellite Routing

Zijun Yang, Sheng Cen and Yifei Zhu
UM-SJTU Joint Institute, Shanghai Jiao Tong University, Shanghai, China
{zijunyang, cens98, yifei.zhu}@sjtu.edu.cn

2025 IEEE/ACM International Symposium on Quality of Service (IWQoS) | 979-8-3315-4940-4/25/$31.00 ©2025 IEEE | DOI: 10.1109/IWQOS65803.2025.11143286

***Abstract*—Low Earth Orbit (LEO) satellite networks, such as Starlink, have become essential complements to terrestrial networks, significantly expanding Internet access in rural areas. However, their robustness in the face of various threats remains largely unexplored. In this paper, we present the first comprehensive study on the impact of four critical factors—direct sunlight, solar superstorms, high workload, and wear and tear—on Inter-Satellite Link (ISL) failures and their effects on network routing performance. We systematically model these failure mechanisms and analyze their influence under three classical routing algorithms. Our evaluation includes both network-wide connectivity and end-user latency analysis. Our findings reveal that LEO satellite networks relying on static routing algorithms are highly vulnerable, whereas dynamic and distributed routing approaches exhibit greater resilience. While multipath routing enhances robustness through redundancy, it encounters two key challenges: throughput bottlenecks and performance degradation under high-latitude traffic loads. In contrast, distributed routing maintains resilience with minimal latency trade-offs. These insights underscore the need for adaptive routing frameworks that integrate spatial redundancy with traffic-aware load balancing to ensure reliable network performance. Code for this paper is available at https://github.com/zpatronus/Robustness-Analysis-of-LEO-Satellite-Routing.**

***Index Terms*—satellite constellations, low Earth orbit satellites, network reliability, routing protocols**

I. Introduction

The advancement of LEO satellite networks has made it a critical component in the coming Internet architecture. Modern LEO satellite networks leverage ISLs to enable routing within the constellation, replacing the traditional bent-pipe architecture that relies on ground relays. By eliminating the zigzag path between satellites and ground relays, ISLs significantly reduce the path length, thereby lowering latency and increasing throughput. Furthermore, ISLs operate on high-frequency bands, which enhance data transmission capacity and contribute to high throughput [17].

Compared with terrestrial networks, LEO satellite networks offer distinct advantages. For instance, they provide connectivity to remote and rural areas where deploying terrestrial infrastructure, such as fiber optics, is economically or geographically challenging [29]. This makes LEO satellite networks the only option for such regions. Additionally, LEO satellite networks can deliver lower latency than terrestrial networks, particularly for transcontinental communication, making them ideal for latency-sensitive applications like stock trading [4]. For example, Starlink, the most successful LEO satellite network to date, has expanded its coverage to over 60 countries and serves more than 1.5 million subscribers [59]. Starlink's low altitude ensures terrestrial-like quality for web browsing and other online activities, particularly in areas where deploying fiber optics is impractical [2], [3], [5]. The median download speed for a single user on Starlink exceeds 100 Mbps, while the median upload speed is around 20 Mbps, comparable to the speeds offered by traditional ISPs to average users [6].

LEO satellites operate in space, a harsh environment where disruptions in LEO satellite networks can lead to significant economic losses. For example, a 2-hour Internet outage in the United States alone can result in losses nearing 1 billion USD [1]. Considering the potential losses and the upcoming emergence of LEO satellite networks as an important part of the global Internet, research on understanding various kinds of threats in depth and analyzing the robustness of the satellite networks across these threats is urgently needed.

However, little is known about the connectivity and latency of LEO satellite networks under such threats so far. Most research on robustness analysis focuses on terrestrial networks [10], [34], [56]. On the other hand, robust analyses on LEO satellite networks have been conducted in an ad hoc approach, with each targeting a specific threat at different layers. For example, at the communication device level, Zhang et al. [8] introduce heterodyne coherent tracking technology to increase the signal-to-noise ratio when laser beams are submerged in direct sunlight. At the computing circuit level, Pfandzelter and Bermbach [11] analyze the rate of on-board computer failures caused by cosmic rays, which may lead to satellite malfunctions. Yan et al. [12] compare error correction codes and triple modular redundancy, two methods for addressing single-bit flips in memory modules. Giuliari et al. [20] explore cyberattacks on satellite networks that can cause congestion. There is no systematic analysis of the impact of various threats on routing performance in the network layer so far.

Therefore, to fill in this gap, we present the first work to systematically analyze how the LEO satellite network will degrade when encountering various kinds of threats posed by the harsh space environment. We classify threats to LEO satellite networks into four categories: direct sunlight, solar superstorm, high workload, and wear and tear. Direct sunlight,

This work is supported by the National Natural Science Foundation of China (Grant No. 62302292). The corresponding author is Yifei Zhu.

referring to unobstructed solar radiation, increases noise in laser systems, reducing their signal-to-noise ratio [8]. Solar superstorms generate intense cosmic rays that penetrate satellite shielding, which can induce single-event upsets, causing bit flips in memory modules [10], [11]. High workload, defined as sustained peak demand exceeding ISL capacity, creates routing bottlenecks that lead to congestion in inter-satellite communications [4]. Wear and tear encompasses cumulative degradation effects from prolonged operation and manufacturing defects in specific component batches [28].

We choose the representative Starlink LEO satellite network as the subject, build models for threat patterns, and simulate the effects of these threats by malfunctioning ISLs in the satellite network accordingly. We then conduct the macroscopic-level connectivity analysis as well as the microscopic user latency analysis under three classical routing algorithms. Insights on routing algorithm design and network management imperatives are concretely discussed. In summary, our contributions and major discoveries are summarized as follows:

- We present the first comprehensive robustness analysis of LEO satellite routing under systematically composed threats.
- We identify that a phase shift (>0.06) is a critical mitigation measure against direct sunlight interference.
- We expose catastrophic vulnerability (near-zero connectivity) of shortest path and multipath routing under high workload scenarios for cities above mid-latitudes within the same hemisphere.
- We quantify wear-and-tear-induced batch failures in aging orbital shells, showing comparable resilience between distributed routing and multipath routing.
- We assess the robustness of different routing algorithms and conclude that the distributed routing algorithm offers superior resilience over others.

The rest of the paper is organized as follows: Section II presents how we model LEO satellite networks. The causes and the patterns of malfunctioning ISLs are analyzed in Section III. In Section IV, we analyze the overall region-to-region connectivity of the satellite network with different routing algorithms and the latency between different city pairs. Related works are reviewed in Section VI , and we conclude this paper in Section VII.

II. Characterizing the LEO satellite network

There has been a rapid increase in the popularity of LEO satellite networks capable of intra-constellation routing. The traditional architecture of satellite networks is bent pipe with the satellites serving as relays between ground stations [5]. In comparison, we focus on the LEO satellite networks with ISL enabled, which can be realized by laser transceivers equipped on LEO satellites [4]. By substituting the zigzag ground-satellite path in the bent pipe architecture with a free-space optical communication path within the constellation, the LEO satellite network can establish connections with reduced latency.

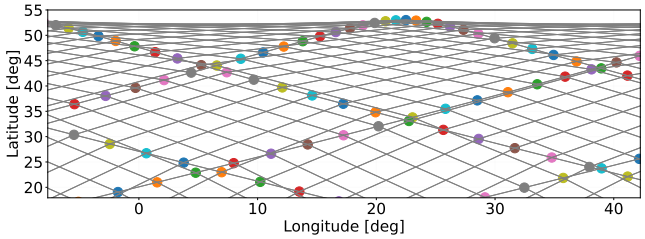

Fig. 1: Starlink under given parameters. The map is zoomed on 0-40° east and 25-53° north to better show the connection between satellites.

Unlike Geostationary Satellite Networks (GSN), LEO satellite networks are closer to the Earth, usually located at 200-3000 km above sea level [5]. The close distance leads to a small round-trip latency of 0.2-20 ms compared to the 100-500 ms latency of a GSN [5]. These satellites, typically around 1 m in diameter, are smaller than traditional ones, with proposals for decimeter-scale versions in development [9], [30]. Their compact size limits solar panel area, constraining energy harvesting, while the use of supercapacitors (instead of lithium batteries) to reduce weight and cost further restricts available energy [9]. Consequently, energy constraints hinder certain methods for enhancing ISL signal-to-noise ratios [9], [10].

An LEO satellite network is defined by multiple parameters. Fig. 1 displays a zoomed-in map of the spatial location of satellites, ISLs and orbital planes of the main shell of Starlink's LEO satellite network, with satellites represented by dots and ISLs by gray lines. Satellites within the same orbital plane are colored the same and connected by ISL. It focuses on regions from 0-40°E and 20-55°N for improved readability. Take the satellite colored cyan at around 14°E and 38°N, for example. It is connected northeast-southwest with two satellites in the same orbit colored cyan, and two satellites in the neighboring orbits, one colored blue and one olive. An LEO satellite network consists of one or several shells, each comprising several orbital planes, which in turn consist of numerous satellites. The orbital planes and satellites within a shell are typically distributed evenly to ensure consistent service over time. Satellites within a shell share the same altitude. There are many ISL patterns. The most common one connects a satellite to the two closest satellites in its orbit, as well as to two satellites in the adjacent orbits. Advanced LEO satellite networks may feature intermittent ISL connections between shells or complex ISL patterns within a single shell to achieve better connectivity.

The inclination is the angle between the orbital plane and the equatorial plane. This is equal to the maximum latitude a satellite can reach, and thus it directly impacts LEO satellite network coverage. As shown in Fig. 1, Starlink's LEO satellite network has an inclination of 53°. Phase shift ϕ indicates the relative position of neighboring orbits. Let (i, j) denote the satellite at position j in the i^{th} orbit. Given ϕ, (i, j) and $(i + 1, j + \phi)$ pass the equator simultaneously, meaning the

TABLE I: Parameters of Starlink's Satellite Network

Parameters	Values
Inclination	53°
Altitude	550 km above sea level
# of ISL per satellite	4
Phase shift	$11/72$
# of orbit	72
# of satellites per orbit	22
Cycle	5731 s

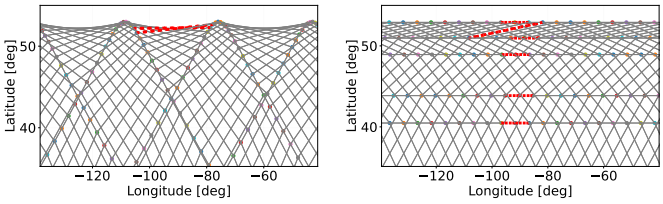

(a) Phase shift of $11/72$ (b) Phase shift of 0

Fig. 2: Constellation affected by direct sunlight around Mar. 21, the Spring Equinox, when the sun is directly over the Earth's equator. Malfunctioning ISLs are shown with red dotted lines. The map is zoomed in to better show the malfunctioning ISL.

neighboring orbits are misaligned by $\frac{2\pi\phi}{\text{\# of satellites per orbit}}$ [4]. A small phase shift results in horizontally close connections between neighboring orbits, facilitating low-latency east-west connections. Conversely, a large phase shift leads to more diagonal connections between neighboring orbits, favoring north-south connections [4], [26], [27].

In this paper, we select Starlink's Group 1 shell as our subject of study, specifically the orbital shell at 550 km altitude with a 53° inclination [17]. Our selection is based on Starlink's status as a widely deployed commercial LEO satellite network with substantial user adoption [2], [6]. The network parameters of Starlink's satellite constellation are detailed in Table I [3], [16], [17]. We adopt a phase shift of $11/72$ for the remainder of this paper. Each Starlink satellite has five pairs of laser transmitters and receivers for ISLs [4]. This study employs only four pairs (connecting (i, j) to $(i, j \pm 1)$ and $(i \pm 1, j)$) [4], [7], excluding the less reliable fifth pair, which experiences shorter connection windows and requires more demanding laser tracking technologies.

III. Threat Analysis and Modeling

In this section, we present an in-depth analysis of how the four potential threat types: direct sunlight, solar superstorm, high workload, and wear and tear affect the ISLs and thus the overall performance of the LEO satellite network.

A. Direct Sunlight

When the angle between the receiving axis of the ISL receiver and the sunlight is less than 3°, the laser signal can be submerged in direct sunlight [8]. There are methods like the Heterodyne Coherent Tracking Technology to improve the signal-to-noise ratio to reduce the impact by direct sunlight, but they come at a cost of more circuit area and draining more power at the receiver or transmitter side. Thus, they may be impractical to be implemented on nano satellites that have other computing missions and limited energy harvesting [8], [9]. For those systems, direct sunlight can be a critical threat and worth analysis.

The vulnerability of LEO satellite networks to direct sunlight is closely linked to their phase shift. As shown in Fig. 2b, satellite networks with a phase shift close to 0 experience more ISL failures due to their parallel and evenly distributed ISLs. Testing reveals that a phase shift greater than 0.06 reduces malfunctioning ISLs caused by direct sunlight to fewer than 10 at any given time for Starlink's satellite network. While this phase shift may compromise east-west connectivity, it significantly improves resilience against sunlight interference, making it a recommended deployment strategy.

We model sunlight as parallel rays. Due to the symmetrical distribution of satellites, direct sunlight creates two clusters of malfunctioning ISLs on opposite sides of the Earth. Fig. 2 illustrates one such cluster during the Spring Equinox. Also, the Earth's terminator is the only place where ISLs can form a small angle with sunlight. For constellations with large phase shifts (e.g., Fig. 2a), malfunctioning ISLs cluster near the high-latitude areas. This is because large phase shifts tilt ISLs in low-latitude regions, preventing alignment with sunlight.

There are seasonal variations in ISL malfunctions, which cluster at high latitudes during the Spring Equinox and migrate toward the equator as the seasons shift toward summer or winter. This movement is modeled based on the angle of sunlight, which varies seasonally. Specifically, the sunlight is directly overhead at the equator during the Spring and Fall Equinoxes, but shifts to a maximum of 23.5° north or south during the Summer and Winter Solstices. This change in the angle of sunlight causes the required alignment angle for ISLs to adjust accordingly, leading to the observed pattern of malfunctions.

B. Solar Superstorm

Solar activities like solar flares and coronal mass ejections (CMEs) impact space electronics. Solar flares emit high-energy particles, while CMEs eject plasma and magnetic fields that expand through space [33], [35], [38]. These phenomena can damage terrestrial electronics despite Earth's protective atmosphere and magnetic field. One notable event occurred in 1859 when the Carrington solar flare caused widespread telegraph system disruptions through induced geomagnetic currents [35], [36].

Satellite network infrastructures are more vulnerable to solar activity than terrestrial electronics due to the absence of protective shielding. Solar superstorms cause bit flips in cache, memory, and storage, resulting in malfunctions in laser components or the entire satellite [10], [11]. On February 4th, 2022, 40 new Starlink satellites were lost due to a surge of plasma from the sun [60]. The solar superstorms would greatly affect the connectivity of satellite networks. According to [10],

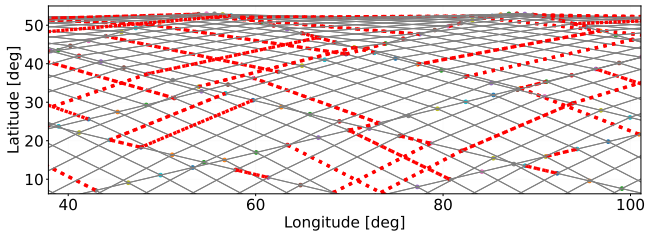

Fig. 3: Constellation affected by solar superstorm with an ISL failure percentage at 15%. Malfunctioning ISLs are shown with red dotted lines. The map is zoomed in to better show the random distribution of malfunctioning ISLs.

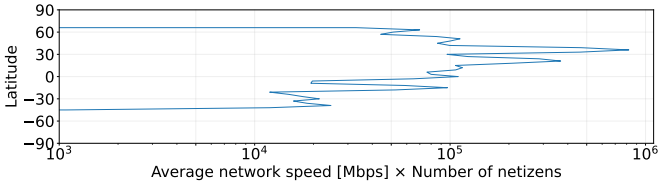

Fig. 4: Estimated traffic distribution with respect to latitude. The traffic is calculated by population×netizen rate×average download speed, which will be discussed in Section IV.

even a 10% failure rate in terrestrial repeaters can lead to over 60% Internet connectivity loss, a level of malfunction that can be more easily reached in the harsh space environment.

Notably, around 2025, satellites may encounter a harsher space environment due to the 11-year solar activity cycle [10], [40]. Consequently, the impacts of a massive solar storm could exceed current expectations, as projections based on existing radiation-level models may underestimate the severity of solar-driven disturbances [10], [41].

Despite methods like thicker shielding, error correction codes, and triple redundant modules being available to tackle this threat, they come at a cost of additional weight, volume, and circuit size and thus a loss of economic efficiency, performance, and an increase in power consumption [11], [12]. Therefore, effectively addressing solar superstorms at low costs remains a significant challenge for the LEO satellite network.

To simulate the impact of solar superstorms through randomly distributed ISL disruptions, we shut down 15% of the total ISLs. For example, when this disruption ratio equals 15%, Fig. 3 illustrates the resulting malfunctioning links.

C. High Workload

In Starlink's network, satellites experience progressively heavier workloads as their operating latitude increases toward the coverage limit of 50° [4]. This operational stress stems from two key factors: (1) the concentration of developed nations between 30-55°N latitude that generate disproportionate traffic volumes, as shown in Fig. 4 [21]; (2) the fundamental geometry of intercontinental data flows.

The intensification of workload at higher latitudes is further exacerbated by routing patterns. In the northern hemisphere,

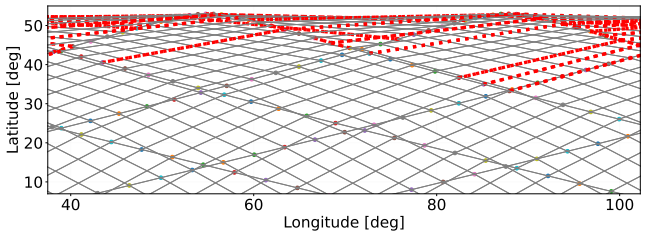

Fig. 5: Constellation affected by high workload. Malfunctioning ISLs are shown with red dotted lines. Functioning ISLs with top 15% latitude have the possibility to fail, and the malfunctioning ISLs count 15% of the total ISLs. The map is zoomed in to better show the distribution of malfunctioning ISLs concentrated at high latitudes.

the shortest great-circle paths between major hubs often traverse polar regions. For instance, when routing algorithms prioritize low latency—a common preference in network design—data packets between Los Angeles and Shanghai are likely to follow high-latitude paths near the Arctic. This routing tendency, combined with existing traffic from densely populated mid-latitude regions, creates critical congestion points above 40°N latitude. While the specific path may vary depending on the routing algorithm, the preference for low latency makes high-latitude routing a common scenario.

As satellite networks expand their user base, traffic growth strains ISLs whose current maximum throughput remains limited to 2.5Gbps [42]–[44] - orders of magnitude below terrestrial cables' 60Tbps capacity [45]–[47]. While load balancing helps alleviate congestion, satellite networks cannot match terrestrial throughput without fundamental ISL technology advancements.

The confluence of traffic concentration, ISL limitations, and thermal stress from sustained operation creates failure risks. Our simulation models these effects through an adaptive threshold mechanism: initial ISL failures occur above a latitude threshold (calculated from orbital inclination and iteration count), then progressively lower this threshold until reaching a target failure count. For example, Fig. 5 shows a possible malfunctioning pattern at a 15% ISL failure rate. This approach replicates how congestion-triggered QoS mechanisms might disable overwhelmed high-latitude ISLs, with failure zones expanding downward as system stress persists.

D. Wear and Tear

Satellite wear-and-tear combines planned retirement and unpredictable failures. Starlink's approach exemplifies this: Each launch deploys 60 satellites across three adjacent orbital planes [13]. These satellites share two failure risks: (1) Synchronized 5-year lifespans [62] mean entire batches approach retirement simultaneously, and (2) Shared manufacturing defects (like automotive batch recalls [48]) could trigger clustered failures. Earlier deployments degrade faster due to cumulative component wear and debris collisions [28].

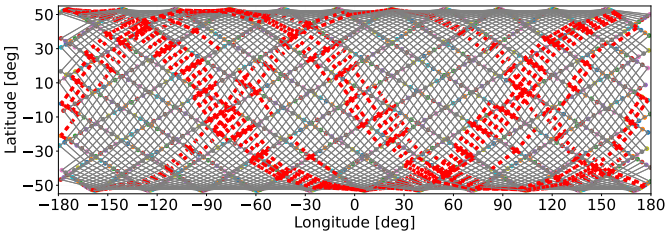

Fig. 6: Constellation affected by wear and tear. Malfunctioning ISLs are shown with red dotted lines. The malfunctioning ISLs are colored red and count 15% of the total ISLs. The ISLs connecting satellites around 180° west and 180° east are hidden for a clean look.

We model these effects using the following rules: When any satellite fails, others from its original 60-satellite launch batch (clustered in three orbital planes) are susceptible to failure next. For example, at a 15% ISL failure rate, Fig. 6 shows how this creates orbital failure rings—defective ISLs from the same batch align along their orbits [13].

IV. The Impact of Threat on Satellite Network's Performance

In this section, we present the analysis details of these four threats, starting with the experiment settings. We then conduct both network-wide and end-user perspective analysis of the network under different routing algorithms.

A. Experiment Setting

Constellation simulation. Existing simulation tools such as Hypatia [7] and StarPerf [3] lack the flexibility to model the dynamic and granular aspects of our satellite network. Moreover, a Python-based simulator would be computationally prohibitive, taking weeks to complete a single run on a standard PC. To achieve the required simulation fidelity and computational efficiency, we developed a custom-built simulator in C++ complemented by Python scripts for data visualization.

Our simulator models the satellite network topology as an undirected graph, where bidirectional communication between satellites is represented by paired laser terminals (vertices) and ISLs as edges. Edge weights correspond to latency, calculated from distances divided by the speed of light in a vacuum. The predictable periodic motion of satellites allows for efficient computation of vertex locations, enabling dynamic updates to edge weights and supporting advanced location-based routing algorithms. Vertices belonging to the same satellite are interconnected with zero-weight edges, assuming latency-free packet forwarding within one satellite [3], [7]. Path costs are determined by cumulative latency along transmission paths. For this study, we exclusively evaluate inter-satellite transmission performance and omit data transmission processes between satellites and ground stations.

Routing algorithms. We evaluate the robustness of three routing algorithms: shortest path [3], multipath [4], and a grid-based distributed routing algorithm [15].

The shortest path algorithm refers to the Discrete-time DV-DVTR algorithm [4], [31], [32], which employs Dijkstra's algorithm to generate routing tables oriented to the smallest latency. While the constellation is dynamic and edge weights vary temporally, the topology remains relatively static over short intervals, enabling this approach.

The multipath algorithm computes two vertex-disjoint paths with the shortest and second-shortest latency for parallel packet transmission [4]. Packets are transmitted through both paths, and any successful delivery is considered a success. Edge-disjointness ensures the selected paths do not share ISLs, though satellites may be shared due to four laser component pairs per satellite [4]. This prioritizes redundancy over throughput compared to the shortest path algorithm.

The distributed routing algorithm forwards packets based on exit location, current satellite position, and neighbor locations [15]. It routes packets to the neighbor closest to the exit. When closer neighbors are unavailable, the algorithm falls back to Manhattan distance minimization on an abstract grid defined by orbital planes and intra-orbit satellite positions [15].

Evaluation metrics. We evaluate the impact from both a macroscopic and a microscopic view. The macroscopic view pertains to how well the LEO satellite network performs as a whole under threats. The malfunction of ISLs due to direct sunlight depends on time and phase shift (as introduced in prior sections), while malfunction caused by solar superstorms, high workload, and wear and tear involves numerous difficult-to-analyze factors.

To simulate real-world traffic scenarios when LEO satellite networks become an alternative option to terrestrial networks, we define the *network activity index* of a region as the product of population, netizen rate and average download speed. Data are obtained from the United Nations, the World Bank, and Ookla Speedtest [21]–[23]. The *traffic index* between two regions is defined as the product of their network activity indexes, which estimates the traffic volume between them.

To represent the severity of incidents caused by these factors, we use the ISL failure percentage, which is the number of failed ISLs divided by the total number of ISLs. For solar superstorm, high workload, and wear and tear scenarios, we simulate the ISL failure percentage from 0% to 100%, disabling ISLs according to the threat types until reaching the percentage target, and simulate the disconnection rate. The *disconnection rate* is calculated as the proportion of the sum of traffic indices for disconnected city pairs relative to the total sum of traffic indices. We use a step size of 0.05% from 0% to 1%, 1% from 1% to 10%, 2% from 10% to 20%, and 5% from 20% to 100%. At each ISL failure percentage, the failed ISL selection and simulation are run 100 times to obtain the average final disconnection rate. This offers an overview of the satellite network's overall robustness concerning threat type, ISL failure percentage, time of year, and routing algorithms used [10].

For the microscopic view, we analyze from an actual user's perspective. We test the latency between three city pairs: New York-Beijing, Paris-Cape Town, and Paris-Sydney [3]. These

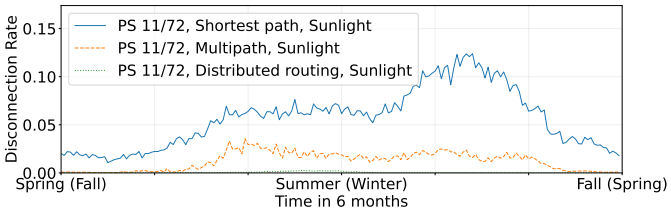

(a) Phase shift of $\frac{11}{72}$

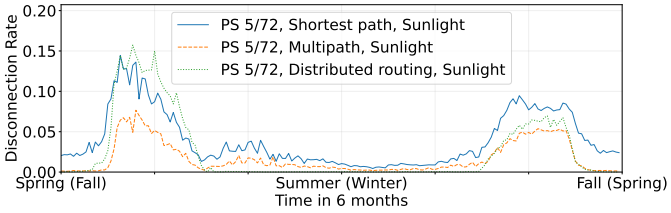

(b) Phase shift of $\frac{5}{72}$

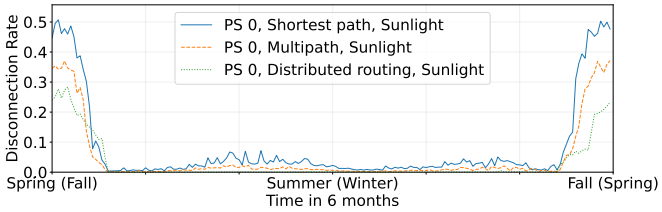

(c) Phase shift of 0

Fig. 7: Region-to-Region disconnection rate over 6 months affected by direct sunlight. The pattern repeats over a period of 6 months.

pairs represent horizontal, vertical, and diagonal connections, respectively. The simulation spans 100 minutes for the solar superstorm and high workload scenario, and 24 hours for the wear and tear scenario (since its pattern manifests only over such long durations). The default ISL failure rate is 15%.

B. Impact of Direct Sunlight

The malfunction of ISLs caused by direct sunlight is only dependent on time given a fixed satellite network configuration. Fig. 7 shows the disconnection rate with respect to time in 6 months of a year from the Spring Equinox to the Fall Equinox (or from the Fall Equinox to next year's Spring Equinox). The pattern has a period of 6 months due to the symmetric layout of the satellite network [8].

The simulation is conducted on Starlink's satellite network with three different phase shifts. The satellite network shown in Fig. 7a has a phase shift of $11/72$, which is the optimal phase shift orienting low latency, and is selected to be tested against the other three kinds of threat: solar superstorm, high workload and wear and tear; the satellite network shown in Fig. 7b has a phase shift of $5/72$ and the one in Fig. 2b has 0 [4]. Comparing the results, it is clear that the peak of disconnection over 6 months is closely related to phase shift: Satellite network with phase shift of 0 and the shortest path algorithm has a stunning 50% disconnection rate around the Equinoxes, while the satellite network with a phase shift of

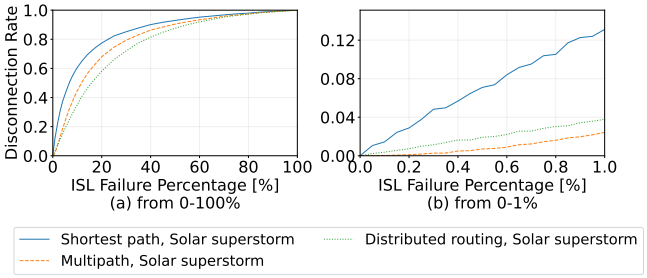

Fig. 8: Region-to-region disconnection rate under solar superstorm with ISL failure percentage from 0-100% and from 0-1%.

$11/72$ only peaks 12.5% with the same routing algorithm. The satellite network with a phase shift of $5/72$ peaks at 15%, which is slightly larger than 12.5% from a phase shift of $11/72$ and significantly lower than 50% from a phase shift of 0, indicating that increasing phase shift helps mitigate the peak of the disconnection rate with a notable marginal effect.

As shown in Fig. 7a, the disconnection rate of the shortest path algorithm reaches a maximum of 12% for approximately two months while exceeding 5% for about six months during a year. This high and persistent disconnection rate is unacceptable for commercial applications. The multipath algorithm improves robustness but still has a disconnection rate of over 2% for six months annually, achieved by halving throughput. The distributed routing algorithm maintains a disconnection rate close to 0 all year with no throughput loss and slightly higher latency, making it suitable for commercial use in Starlink's satellite network with a phase shift of $11/72$. However, for LEO satellite networks with a smaller phase shift and higher ISL failure percentage, the distributed routing algorithm may not perform better, as shown in Fig. 7b. This is because when an LEO satellite network has a small phase shift, several ISLs in the same direction around the Earth's terminator are down at the same time.

From a microscopic point of view, the effects of sunlight on localized areas can be more severe than they appear in the overall region-to-region assessment [8]. Sunlight can cause continuous and complete communication disruptions in certain areas for up to 24 minutes until the rotation of the earth shifts the ISLs out of the angle of interference [8].

C. Impact of Solar Superstorm

Fig. 8 shows the region-to-region disconnection rate with respect to ISL failure percentage under the impact of a solar superstorm. Fig. 8b is an enlarged version of Fig. 8a, specifically focused on the 0-1% range of ISL failure percentage. This magnification provides a clearer depiction of the satellite network's robustness under less extreme conditions.

In the satellite network with the shortest path algorithm shown in Fig. 8, a 1% failure in ISL results in a 12% disconnection rate, escalating to 80% at 20% failure. The satellite network utilizing the multipath algorithm exhibits a 3% disconnection rate at 1% ISL failure, while the distributed

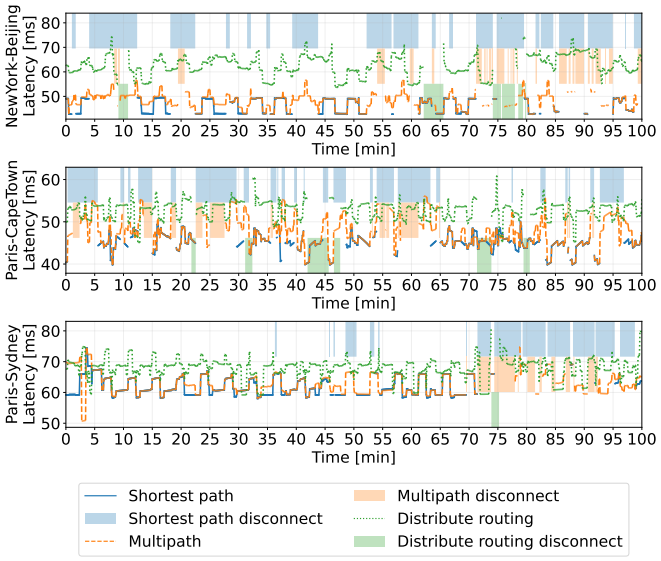

Fig. 9: Latency between city pairs under solar superstorm with ISL failure percentage=5% over 100 minutes.

routing algorithm experiences a 4% disconnection rate under the same conditions. These rates are significantly lower than the disconnection rate observed in the satellite network employing the shortest path algorithm. However, disconnection rates for both satellite networks rise sharply as the ISL failure percentage escalates, reaching 80% for the multipath algorithm at 30% failure and 80% for the distributed routing algorithm at 40% failure.

To further microscopically reveal the user experience affected by the superstorm, we analyze the latency for three different city pairs, depicted in Fig. 9. Under a 5% ISL failure following the solar superstorm impact pattern, latency between three city pairs—New York-Beijing (horizontal connection), Paris-Cape Town (vertical connection), and Paris-Sydney (diagonal connection)—is tested over a 100-minute period. Disconnected intervals are indicated by colored backgrounds corresponding to the routing algorithm. Within each subplot, from top to bottom, the colored bands represent disconnection periods for the shortest path, multipath, and distributed routing algorithms, respectively.

As shown in Fig. 9, the satellite network with the distributed routing algorithm has the lowest total disconnection time among the three algorithms. However, its latency is 10-20 ms higher than that of the other two algorithms. Since the multipath algorithm is based on the shortest path algorithm, they have the same latency most of the time, and the shutdown period of the multipath algorithm is strictly included in that of the shortest path algorithm.

The solar superstorm disrupts ISLs randomly, resulting in an unpredictable distribution of disconnection periods for city pairs. As observed in the simulation, horizontal and vertical connections in the satellite network with the shortest path algorithm experience 5-15 minutes of disconnection periods, while diagonal connections face significantly longer outages of

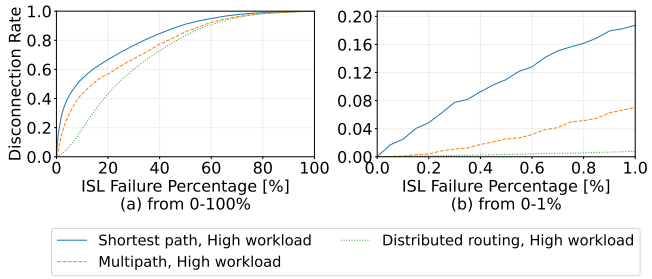

Fig. 10: Region-to-region disconnection rate under high workload with ISL failure percentage from 0-100% and from 0-1%.

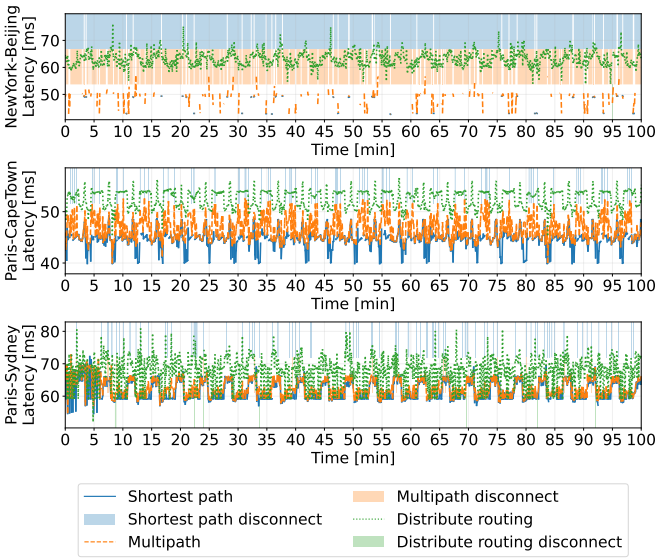

Fig. 11: Latency between city pairs under high workload with ISL failure percentage=5% over 100 minutes.

30-60 minutes. This discrepancy arises because satellites with malfunctioning ISLs require different durations to move out of their orbital positions relative to the desired path. Specifically, diagonal connections sustain prolonged disconnections due to the combined effects of the constellation's inherent phase shift and the geometric alignment requirements of diagonal ISLs. In contrast, horizontal and vertical connections benefit from shorter orbital repositioning periods, though this comes at the cost of more frequent (albeit brief) disconnection events. The distributed routing algorithm demonstrates superior robustness against solar superstorms due to its decentralized path selection, followed by the multipath algorithm leveraging redundant connections, while the shortest path algorithm remains most vulnerable to cascading ISL failures.

D. Impact of High Workload

Fig. 10 illustrates the relationship between the disconnection rate of regions and the ISL failure percentage during high workload conditions. At the 1% ISL failure percentage, the disconnection rates of high workloads with the shortest path and multipath algorithms are 18% and 7% higher than that

of solar superstorms, respectively. However, the distributed routing algorithm exhibits a decrease in the disconnection rate from 4% to 1% under high workload compared to the solar superstorm scenario. This observation emphasizes the dependence of shortest-path-based algorithms on high-latitude ISLs, as discussed in Section III-C. High latitude regions not only tend to cluster with the main traffic-generating regions in the satellite network but also play a crucial role in establishing connections between two mid-latitude areas following the Earth's circumference. Conversely, the distributed routing algorithm intelligently avoids entering malfunctioning high-latitude areas whenever possible, ensuring a low disconnection rate and enhanced resilience.

The disconnection rate of all three routing algorithms rises sharply, reaching up to 80% as the ISL failure percentage grows. Reaching this disconnection level requires a 35% ISL failure percentage for the shortest path algorithm, 43% for the multipath algorithm, and 47% for the distributed routing algorithm. This trend mirrors the solar superstorm scenario; however, the disconnection rate increases more gradually under high workload conditions due to the uneven distribution of failed ISLs. This gradual increase is also evident for the distributed routing algorithm, as illustrated in Fig. 10a. Therefore, compared with the other two algorithms, the distributed routing algorithm demonstrates higher resilience to ISL failures, particularly at lower failure percentages.

Fig. 11 illustrates the latency experienced by users under the impact of high workload and a 5% ISL failure percentage. The result affirms the vulnerability of high-latitude regions in satellite networks employing a shortest-path-based algorithm under high workload impact. Both New York and Beijing, situated at a latitude of 40 N, are geographically distant from each other. Consequently, the shortest path connecting these cities is likely to traverse high-latitude ISLs, resulting in a near-complete disconnection between them throughout the entire 100-minute period when utilizing the shortest path and multipath algorithms. However, employing the distributed routing algorithm completely mitigates this disconnection, albeit at the expense of a 15 ms increase in latency. On the other hand, the other two city pairs, Paris-Cape Town and Paris-Sydney, exhibit lower disconnection due to the infrequent utilization of high-latitude ISLs in the paths determined by all three algorithms. In summary, the distributed routing algorithm demonstrates superior robustness against high workload-induced ISL failures by strategically bypassing vulnerable high-latitude regions, while shortest-path-based algorithms remain constrained by their inherent dependence on these critical yet failure-prone ISLs.

E. Impact of Wear and Tear

Fig. 12 shows the region-to-region disconnection rate with respect to the ISL failure percentage under the impact of wear and tear. When the ISL failure percentage is at 1%, the satellite network employing the shortest path algorithm exhibits a disconnection rate of 8%, while the multipath and distributed routing algorithms demonstrate disconnection rates of 3% and

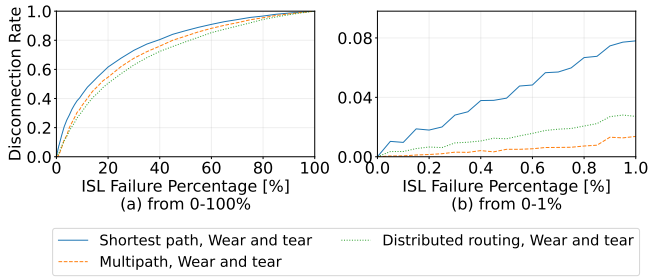

Fig. 12: Region-to-region disconnection rate under wear and tear with ISL failure percentage from 0-100% and from 0-1%.

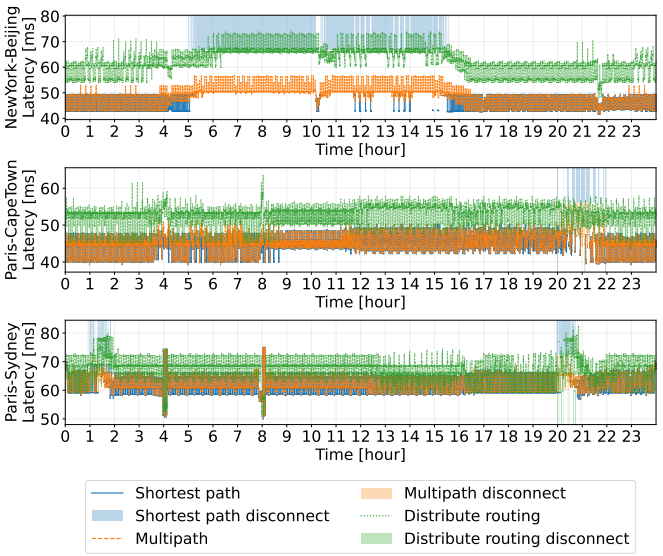

Fig. 13: Latency between city pairs under wear and tear with ISL failure percentage=5% over 24 hours.

1.5%, respectively. The observed relative robustness of these three routing algorithms aligns with the findings obtained in the preceding two subsections.

As the ISL failure percentage rises, the disconnection rate also increases rapidly, eventually reaching an 80% disconnection rate at approximately 43% ISL failure percentage. Despite the shortest path algorithm exhibiting the poorest robustness and the distributed routing algorithm demonstrating the highest, the disparity in disconnection rates among the three algorithms for the same ISL failure percentage is small, even within a low ISL failure range. This implies that when confronted with wear and tear, the ability of the multipath and distributed routing algorithms to mitigate such disruptions is limited.

Fig. 13 illustrates the latency experienced among three city pairs over a 24-hour period, considering the impact of wear and tear and an ISL failure percentage of 5%. The chosen duration of 24 hours aligns with the Earth's rotation period, which directly impacts the latency and connectivity experienced by actual users in the wear and tear scenario. Unlike the random and intermittent nature of disconnections

under solar superstorms, the disconnection periods caused by wear and tear are continuous and can last for several hours. This is particularly true for connections involving high-latitude regions, such as New York and Beijing, where the path connecting them coincides with the trajectory of malfunctioning satellites, resulting in disconnections until these satellites have passed. The vertical and diagonal connections experience much less disruption. Overall, the distributed routing algorithm remains the most robust against wear and tear due to its dynamic path adjustments, followed by multipath routing's redundancy and shortest path's rigidity, but their effectiveness diminishes significantly as satellite failures persist over time.

V. Discussion and Guidelines

Our analysis of three routing algorithms (shortest path, multipath and distributed) under four distinct threats to LEO satellite networks reveals critical insights into network robustness. Below, we synthesize these findings to guide mitigation strategies.

Direct sunlight interference demands larger phase shifts in LEO satellite networks to minimize disconnections caused by thermal expansion. By anticipating peak disconnection moments, operators can strategically adjust orbital parameters. Mitigation strategies should balance network robustness with energy efficiency and throughput: for instance, increasing ISL transmission power improves SNR but raises energy consumption. The distributed routing algorithm excels here, achieving zero disconnections with optimal phase shifts by dynamically adapting to sunlight-induced link variations.

Solar superstorms induce unpredictable ISL disruptions. While centralized routing struggles with rapid topology changes, distributed and multipath algorithms maintain robustness at low ISL failure rates. This resilience stems from their ability to implement dynamic rerouting—non-concentrated, intermittent failures allow these algorithms to bypass damaged links in real time, unlike shortest-path-based approaches that rely on fixed routes.

High workload strain disproportionately affects high-latitude ISLs due to polar traffic convergence. Distributed routing outperforms alternatives at low failure rates by autonomously redistributing traffic across adjacent nodes, preventing localized congestion. Implementing load balancing technologies could further alleviate strain.

Hardware wear and tear causes batch-level satellite failures, encompassing both scheduled retirement (predictable aging) and unscheduled defects (e.g., manufacturing flaws). Scheduled retirement allows proactive measures like deploying replacements before degradation. For unpredictable manufacturing defects, multipath and distributed routing leverage path redundancy to mitigate low failure rates.

The shortest path algorithm is highly vulnerable to all threat types due to its static path dependencies, with single ISL failures potentially causing widespread disconnections. Multipath routing enhances resilience through redundancy but suffers from throughput limitations and persistent disconnections in the high-workload scenario. Distributed routing offers superior adaptability by dynamically avoiding failures, albeit with a slight latency increase.

VI. Related Works

Modeling LEO Satellite Networks. Lai et al. [3] and Kassing et al. [7] develop simulators for characterizing LEO satellite networks, while SpaceX's FCC filings [16], [17] detail orbital parameters affecting network performance. Handley [4] proposes low-latency inter-satellite link (ISL) patterns and hybrid ground-space relay architectures. McDowell [13] provides operational deployment insights through Starlink launch tracking. Connection dynamics between ground stations and satellites are examined by Michel et al. [2] and Hu et al. [5].

Routing in LEO Satellite Networks. Handley [4] introduces multipath routing using disjoint paths, while Ekici et al. [15] develop distributed routing algorithms for dynamic topologies. Li et al. [24] propose geospatial addressing schemes, and Giuliari et al. [18] advocate path-aware networking alternatives to BGP. Bhosale et al. [25] analyze latency-throughput tradeoffs in variable constellations.

Threats Analysis in Space Systems. Zhang et al. [8] identify sunlight interference challenges for laser links, while Jyothi [10] analyzes solar storm risks to satellite electronics. Radiation-induced errors are mitigated through Pfandzelter et al.'s fault-tolerance framework [11] and Yan et al.'s neural network hardening [12]. Giuliari et al. [20] demonstrate practical DDoS vulnerabilities in LEO constellations. Guo et al. [51] develop comprehensive failure models for integrated space-air-ground networks, categorizing failures by component type and spatial scale.

In contrast to these studies, we systematically investigate LEO satellite networks under adversarial space conditions. Our work characterizes threat-induced ISL failure patterns and evaluates routing algorithm resilience across diverse threat scenarios, bridging the gap between isolated threat analyses and network robustness quantification.

VII. Conclusion

The robustness of LEO satellite networks under diverse space-environment threats remained poorly understood. In this paper, we systematically analyzed four critical threats—direct sunlight, solar superstorms, high workload, and wear-and-tear—and their impacts on routing performance through large-scale simulations. By evaluating network-wide connectivity and end-user latency under three routing algorithms, we revealed that static shortest-path routing is highly vulnerable, while dynamic distributed routing exhibits superior resilience. Multipath routing mitigates disruptions via redundancy but struggles with throughput bottlenecks and high-latitude congestion. Our study underscores the importance of phase-shift optimization to counter sunlight interference, adaptive rerouting for cosmic-ray-induced failures, and proactive load-balancing to alleviate high-latitude traffic strain, and strategic replacement plans to counteract satellite aging at the batch level. This work provides insights for designing robust LEO

satellite networks and inspires adaptive frameworks to safeguard future satellite infrastructures.

REFERENCES

[1] NetBlocks® cost of shutdown tool. https://netblocks.org/cost/.

[2] F. Michel, M. Trevisan, D. Giordano, and O. Bonaventure. A first look at Starlink Performance, in *Proc. ACM IMC*, 2022.

[3] Z. Lai, H. Li, and J. Li. StarPerf: Characterizing network performance for emerging mega-constellations, in *Proc. IEEE ICNP*, 2020.

[4] M. Handley. Delay is not an option, in *Proc. ACM HotNets*, 2018.

[5] Y. Hu, and V. O. K. Li. Satellite-based internet: A tutorial. *IEEE Communications Magazine*, vol. 39, no. 3, pp. 154–162, 2001.

[6] J. Fomon. Starlink resurgence? speeds increase in Europe and Oceania: Ookla. https://tinyurl.com/2mh4ttky.

[7] S. Kassing, D. Bhattacherjee, A. B. Águas, J. E. Saethre, and A. Singla. Exploring the 'internet from space' with Hypatia, in *Proc. ACM IMC*, 2020.

[8] W. Zhang, X. Yan, C. Cao, X. Zeng, Z. Feng, C. Jiang, B. Wang, and R. Zhang. Heterodyne coherent tracking technology for inter-satellite laser link during direct sunlight. *Infrared Physics & Technology*, vol. 116, p. 103817, 2021.

[9] B. Denby, and B. Lucia. Orbital edge computing: Nanosatellite Constellations as a New Class of Computer System, in *Proc. ACM ASPLOS*, 2020.

[10] S. A. Jyothi. Solar Superstorms: Planning for an Internet Apocalypse, in *Proc. ACM SIGCOMM*, 2021.

[11] T. Pfandzelter and D. Bermbach. Failure is not an Option: Considerations for Software Fault-Tolerance in LEO Satellite Edge Computing. *CoRR*, vol. abs/2302.08952, 2023.

[12] Z. Yan, Y. Shi, W. Liao, M. Hashimoto, X. Zhou, and C. Zhuo. When single event upset meets Deep Neural Networks: Observations, explorations, and remedies, in *Proc. IEEE ASP-DAC*, 2020.

[13] J. McDowell. Jonathan's Space Report | Space Statistics. https://planet4589.org/space/con/star/stats.html.

[14] M. Handley. Using ground relays for low-latency wide-area routing in megaconstellations, in *Proc. ACM Hotnets*, 2019.

[15] E. Ekici, I. F. Akyildiz, and M. D. Bender. A distributed routing algorithm for Datagram Traffic in Leo satellite networks. *IEEE/ACM Transactions on Networking*, vol. 9, no. 2, pp. 137–147, 2001.

[16] SpaceX. SpaceX Non-Geostationary Satellite System. https://fcc.report/IBFS/SAT-LOA-20161115-00118/1158350.pdf, 2016.

[17] SpaceX. SpaceX Non-Geostationary Satellite System, modification on satellite space station filing. https://tinyurl.com/556yfxth, 2019.

[18] G. Giuliari, T. Klenze, M. Legner, D. Basin, A. Perrig, and A. Singla. Internet backbones in Space. *ACM SIGCOMM Computer Communication Review*, vol. 50, no. 1, pp. 25–37, 2020.

[19] T. Klenze, G. Giuliari, C. Pappas, A. Perrig, and D. Basin. Networking in heaven as on Earth, in *Proc. ACM HotNets*, 2018.

[20] G. Giuliari, T. Ciussani, A. Perrig, and A. Singla. ICARUS: Attacking low Earth orbit satellite networks, in *Proc. USENIX ATC*, 2021.

[21] United Nation. World urbanization prospects - population division. United Nations. https://population.un.org/wup/.

[22] Ookla. Internet speed around the world. https://tinyurl.com/537s7bxr.

[23] World Bank. Individuals using the internet (% of population). https://data.worldbank.org/indicator/IT.NET.USER.ZS.

[24] Y. Li, H. Li, W. Liu, L. Liu, Y. Chen, J. Wu, Q. Wu, J. Liu, and Z. Lai. A Case for Stateless Mobile Core Network Functions in Space, in *Proc. ACM SIGCOMM*, 2022.

[25] V. Bhosale, A. Saeed, K. Bhardwaj, and A. Gavrilovska. A characterization of route variability in Leo satellite networks. *Passive and Active Measurement*, pp. 313–342, 2023.

[26] D. Bhattacherjee. Towards Performant Networking from Low-Earth Orbit. *Ph.D. thesis, ETH Zurich*, 2021.

[27] SpaceX. Space exploration holdings modification of Ku Ka-band License. https://docs.fcc.gov/public/attachments/DOC-409426A1.pdf.

[28] A. K. Majumdar. Impact and Issues of Existing and Planned Large Satellite Constellation for Communications. *Laser communication with Constellation Satellites, uavs, haps and balloons: Fundamentals and Systems Analysis for Global Connectivity*, pp. 255–258, 2022.

[29] T. Ahmmed, A. Alidadi, Z. Zhang, A. U. Chaudhry, and H. Yanikomeroglu. The Digital Divide in Canada and the Role of LEO Satellites in Bridging the Gap. *IEEE Communications Magazine*, vol. 60, no. 6, pp. 24–30, 2022.

[30] Damir. Starlink Satellite Dimension Estimates. https://lilibots.blogspot.com/2020/04/starlink-satellite-dimension-estimates.html.

[31] X. Qi, J. Ma, D. Wu, L. Liu, and S. Hu. A survey of routing techniques for satellite networks. *Journal of Communications and Information Networks*, vol. 1, no. 4, pp. 66–85, 2016.

[32] X. Cao, Y. Li, X. Xiong, and J. Wang. Dynamic routings in satellite networks: An overview. *Sensors*, vol. 22, no. 12, p. 4552, 2022.

[33] H. Zell. What is a solar flare. https://tinyurl.com/28c37t7f.

[34] V. Luconi and A. Vecchio. Impact of the first months of war on routing and latency in Ukraine. *Computer Networks*, vol. 224, p. 109596, Apr. 2023. https://doi.org/10.1016/j.comnet.2023.109596.

[35] L. W. Townsend, D.L Stephens Jr., J.L. Hoff, E.N. Zapp, H.M. Moussa, T.M. Miller, C.E. Campbell, and T.F. Nichols. The Carrington event: Possible doses to crews in space from a comparable event. *Advances in Space Research*, vol. 38, no. 2, pp. 226–231, 2006.

[36] D. Dobrijevic, and A. May. The Carrington Event: History's greatest solar storm. https://www.space.com/the-carrington-event.

[37] U.S. Geological Survey. Remembering the Great Halloween Solar Storms. https://ncei.noaa.gov/news/great-halloween-solar-storm-2003.

[38] National Oceanic and Atmospheric Administration. Coronal mass ejections. https://www.swpc.noaa.gov/phenomena/coronal-mass-ejections.

[39] NASA. The Day the Sun Brought Darkness. https://www.nasa.gov/topics/earth/features/sun_darkness.html.

[40] NASA. What Is the Solar Cycle? https://tinyurl.com/4hpd5wxb.

[41] Petrovay, K. Solar cycle prediction. *Living Rev Sol Phys 17*, 2020.

[42] Tesat's laser product. https://www.tesat.de/products#laser.

[43] Mynaric's laser product. https://mynaric.com/products/space/.

[44] Optical ISL from General Atomics. https://tinyurl.com/bdddy2rh.

[45] W. Qiu. Hibernia Atlantic Trials the First 100G Transatlantic. https://tinyurl.com/243d86s3.

[46] Antonio. Submarine Cable Repeaters. https://tinyurl.com/wrrk6p8u.

[47] ENC. A Global Consortium to Build New Trans-Pacific Cable System "FASTER". https://tinyurl.com/48n9e6dr.

[48] K. Allen, and J. Sturcke. Toyota's recall woes. https://theguardian.com/business/2010/jan/29/timeline-toyota-recall-accelerator-pedal.

[49] J. Bao, B. Zhao, W. Yu, Z. Feng, C. Wu, and Z. Gong. OpenSAN: A Software-defined Satellite Network Architecture, in *Proc. ACM SIGCOMM*, 2014.

[50] T. Li, H. Zhou, H. Luo and S. Yu. SERvICE: A Software Defined Framework for Integrated Space-Terrestrial Satellite Communication. *IEEE Transactions on Mobile Computing*, vol. 17, no. 3, pp. 703-716, 2018.

[51] X. Guo, L. Ma, W. Su, and X. Jiang. Failure Models for Space-Air-Ground Integrated Networks, in *Proc. IEEE SAT-NET*, 2024.

[52] G. Siganos, and M. Faloutsos. Neighborhood Watch for Internet Routing: Can We Improve the Robustness of Internet Routing Today?, in *Proc. IEEE INFOCOM*, 2007.

[53] A. Marder, Z. Zhang, R. Mok, R. Padmanabhan, B. Huffaker, M. Luckie, A. Dainotti, kc claffy, A. C. Snoeren, and A. Schulman. Access Denied: Assessing Physical Risks to Internet Access Networks, in *Proc. USENIX Security*, 2023.

[54] F. Long. Satellite Network Robust QoS-aware Routing. Springer Berlin, Heidelberg, 2014.

[55] M.S. Hossain, S.S. Hassan, M. Atiquzzaman, W. Ivancic. Survivability and scalability of space networks: a survey. *Telecommun Syst*, vol. 68, pp. 295–318, 2018.

[56] J. Oostenbrink, and F. Kuipers. A Global Study of the Risk of Earthquakes to IXPs, in *Proc. IEEE IFIP Networking)*, 2022.

[57] A. Ramanathan, R. Sankaran, and S. A. Jyothi. Xaminer: An Internet Cross-Layer Resilience Analysis Tool. *Proceedings of the ACM on Measurement and Analysis of Computing Systems*, vol. 8, no. 1, pp. 1–37, 2024.

[58] Starlink. Starlink is now available in Malawi! https://twitter.com/Starlink/status/1683897037639790592.

[59] Starlink. Thank you to our 1.5M+ customers around the world! https://twitter.com/Starlink/status/1654673695007457280.

[60] J. O'Callaghan. SpaceX just lost 40 satellites to a geomagnetic storm. There could be worse to come. *MIT Tech Review*. https://tinyurl.com/j3anmye7.

[61] M. Frąckiewicz. The Role of Starlink in Bridging the Digital Divide. https://ts2.space/en/the-role-of-starlink-in-bridging-the-digital-divide/.

[62] A. Lemole. SpaceX launches first Starlink mission of 2021. https://nasaspaceflight.com/2021/01/spacex-launch-first-starlink-mission-2021/.